J/ψ Production in Cold Nuclear Matter

R. Vogt

Lawrence Livermore National Laboratory, Livermore, CA 94551, USA
Physics Department, University of California, Davis, CA 95616, USA

Production in pp Collisions

Large Uncertainties with FONLL Fiducial Parameters

With a given PDF set define a fiducial region of mass and scale that should encompass the true value – central mass and scale $(m, \mu_F/m, \mu_R/m) = (1.5\,\mathrm{GeV}, 1, 1)$:

- **For $\mu_F = \mu_R = m$, vary mass, $1.3 < m < 1.7$;**
- **For $m = 1.5$ GeV, vary scales independently within a factor of two: $(\mu_F/m, \mu_R/m) = (1, 1)$, (2,2), (0.5,0.5), (0.5,1), (1,0.5), (1,2), (2,1).**

Low scales set limits on uncertainty ($\mu_R/m = 0.5$ upper limt, $\mu_F/m = 0.5$ lower limit)
Large combination of mass and scale uncertainty makes lower limit ill defined

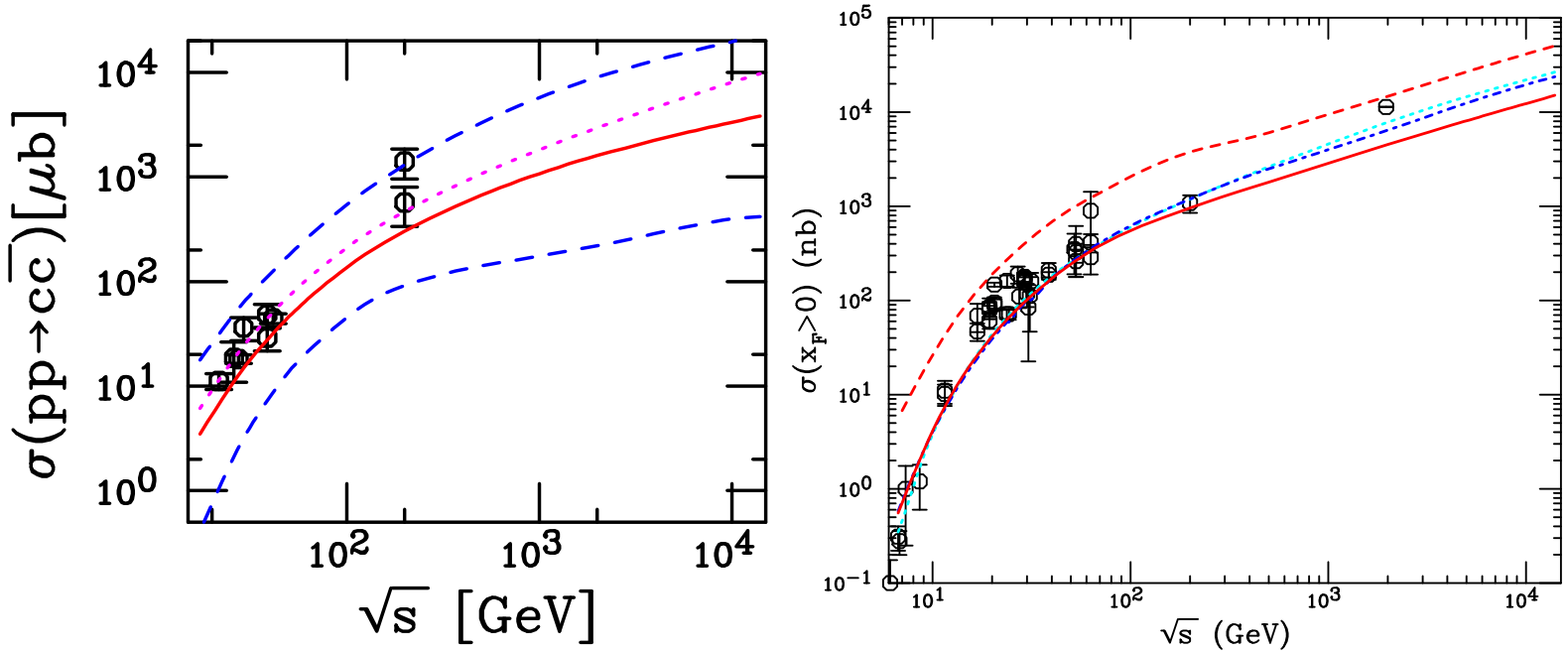

Figure 1: (Left) Uncertainty band formed from adding mass and scale uncertainties in quadrature. (Right) The solid and dashed red curves are the central value and upper limit for the J/ψ cross section. The solid cyan curve employs the MRST HO distributions while the dot-dashed blue curve is a result with CTEQ6M, both employing $m_c = 1.2$ GeV. $(\mu_F/m_T, \mu_R/m_T) = (2, 2)$.

Pinning Down Open Charm Uncertainties by Fitting $\sigma_{c\overline{c}}$

Caveat: full NNLO cross section unknown, could still be large corrections which lead to different results

Employ $m = 1.27$ GeV, lattice value at $m(3\,\mathrm{GeV})$

Use subset of $c\overline{c}$ total cross section data to fix best fit values of μ_F/m and μ_R/m

Result with $\Delta\chi^2 = 1$ gives uncertainty on scale parameters; $\Delta\chi^2 = 2.3$ gives one standard deviation on total cross section

LHC results from ALICE agrees well even though not included in the fits

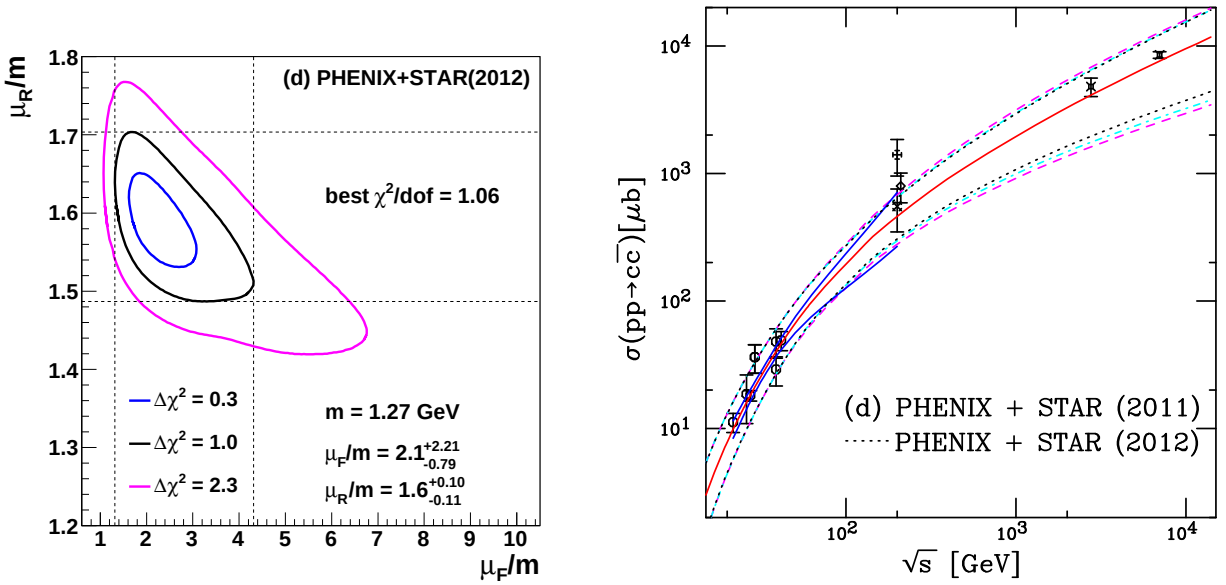

Figure 2: (Left) The χ^2/dof contours for fits including the STAR 2011 cross section but excluding the STAR 2004 cross section. The best fit values are given for the furthest extent of the $\Delta\chi^2 = 1$ contours. (Right) The energy dependence of the charm total cross section compared to data. The best fit values are given for the furthest extent of the $\Delta\chi^2 = 1$ contours. The central value of the fit in each case is given by the solid red curve while the dashed magenta curves and dot-dashed cyan curves show the extent of the corresponding uncertainty bands. The dashed curves outline the most extreme limits of the band. In addition, the dotted black curves show the uncertainty bands obtained with the 2012 STAR results while the solid blue curves in the range $19.4 \leq \sqrt{s} \leq 200$ GeV represent the uncertainty obtained from the extent of the $\Delta\chi^2 = 2.3$ contour.

Results on LHC Heavy Flavor Distributions

Excellent agreement with $\sqrt{s} = 7$ TeV ALICE pp data on muons in the forward region $(2.5 < y < 4)$

Leptons from semi-leptonic heavy flavor decays include contributions from $D \to \mu X$, $B \to \mu X$, $B \to D \to \mu X$, all with $\sim 10\%$ decay branching ratios

Exchanging fit results with results based on $m = 1.5$ GeV gives narrower uncertainty without reducing agreement with data

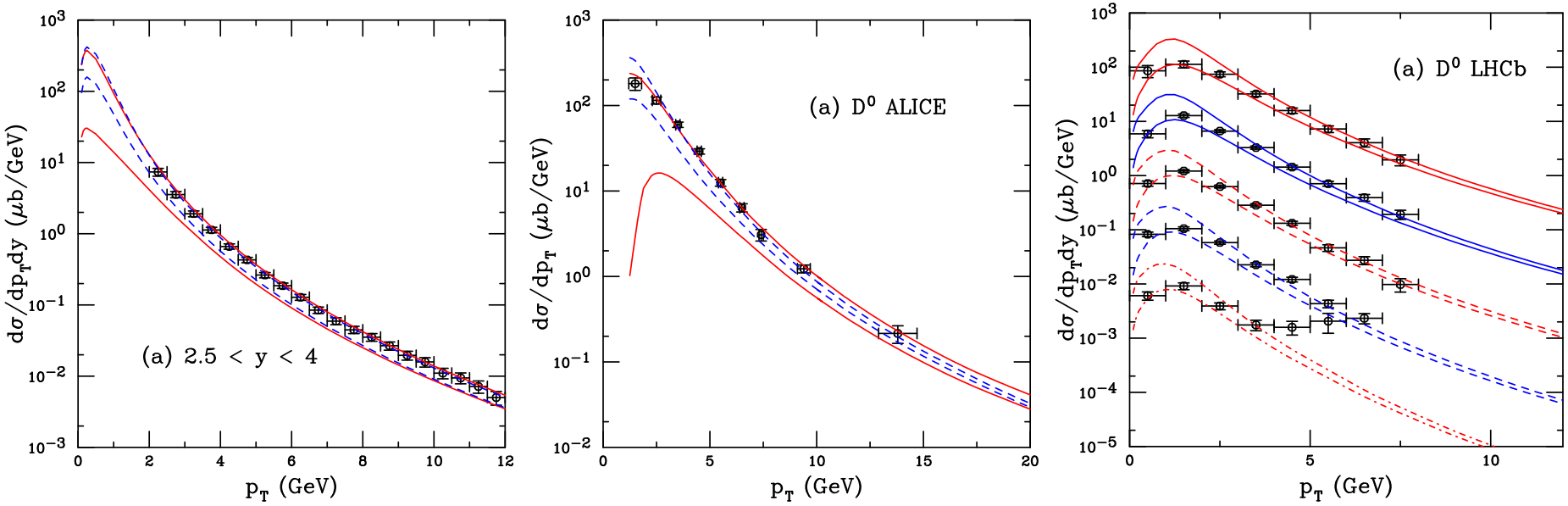

Figure 3: (Left) Comparison of the single lepton p_T distributions in the rapidity interval $2.5 < y < 4$ at $\sqrt{s} = 7$ TeV calculated with the FONLL set for charm (solid red) and the fitted set with $m = 1.27$ GeV (dashed black). (Center) Our calculations are compared with the reconstructed ALICE D^0 data in $|y| \leq 0.5$. The FONLL uncertainty bands with the fiducial charm parameter set are shown by the red solid curves while the blue dashed curves are calculated with the charm fit parameters. (Right) Our calculations are compared with the reconstructed LHCb D^0 data in the rapidity intervals: $2 < y < 2.5$ (solid red); $2.5 < y < 3$ (solid blue); $3 < y < 3.5$ (dashed red); $3.5 < y < 4$ (dashed blue); and $4 < y < 4.5$ (dot-dashed red). The rapidity intervals are separated by a factor of 10 to facilitate comparison. The lowest rapidity interval, $2 < y < 2.5$, is not scaled.

J/ψ Cross Sections from $c\bar{c}$ Fits

Take results of $c\bar{c}$ fits, calculate NLO J/ψ cross section in CEM, fit scale factor F_C (needed to match the $c\bar{c}$ cross section below the $D\overline{D}$ threshold to the inclusive J/ψ cross section) with central value of parameter sets – tighter uncertainty band

CEM calculation reproduces shape of J/ψ p_T and y distributions rather well with single parameter

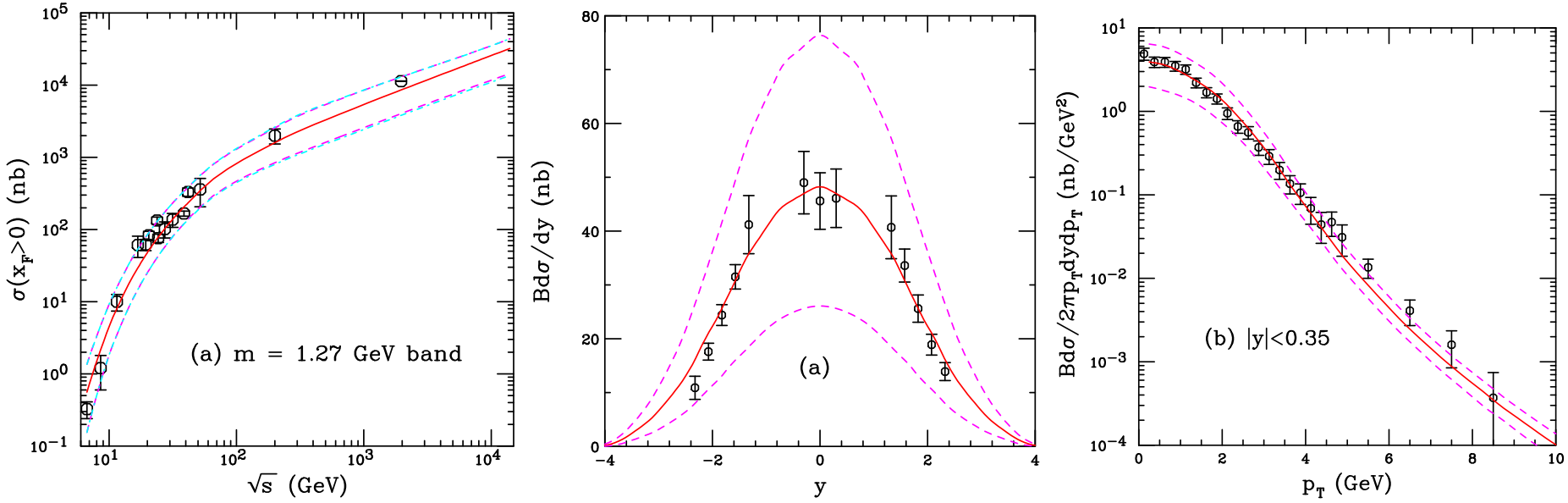

Figure 4: (Left) The uncertainty band on the forward J/ψ cross section. The dashed magenta curves and dot-dashed cyan curves show the extent of the corresponding uncertainty bands. The dashed curves outline the most extreme limits of the band. The J/ψ rapidity distribution (center) and the midrapidity p_T distributions (right) and their uncertainties. The results are compared to PHENIX pp measurements at $\sqrt{s} = 200$ GeV. The solid red curve shows the central value while the dashed magenta curves outline the uncertainty band. A $\langle k_T^2 \rangle$ kick of 1.19 GeV^2 is applied to the p_T distributions

New Calculations in Progress for $b\overline{b}$ and Υ

A Dependence of Open Charm and Quarkonium

Open charm appears to be independent of A ($N_{\rm bin}$) but note that the measurement is at midrapidity only

Definite A dependence for quarkonium while Drell-Yan is effectively independent of A

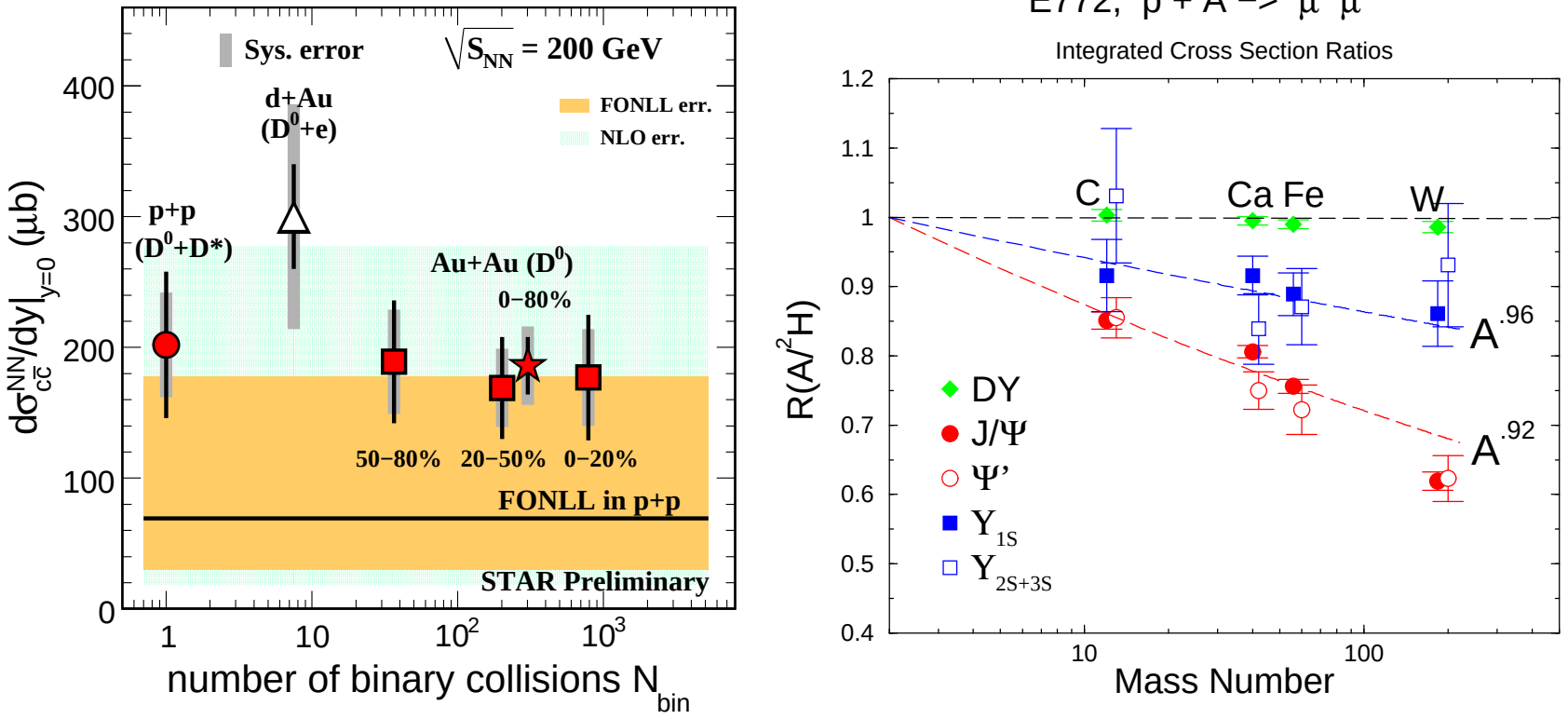

Figure 5: **(Left) The dependence of the open charm cross section on the number of binary collisions measured by the STAR Collaboration at central rapidity. (Right) The A dependence of quarkonium and Drell-Yan production measured by E772.**

E866 Measured Open Charm and J/ψ vs x_F

E866 also measured open charm pA dependence using single muons with $p_T^\mu > 1$ GeV/c (unpublished)

Different from J/ψ for $y < 0.7$ but similar for higher y, suggests that dominant effects are in the initial state

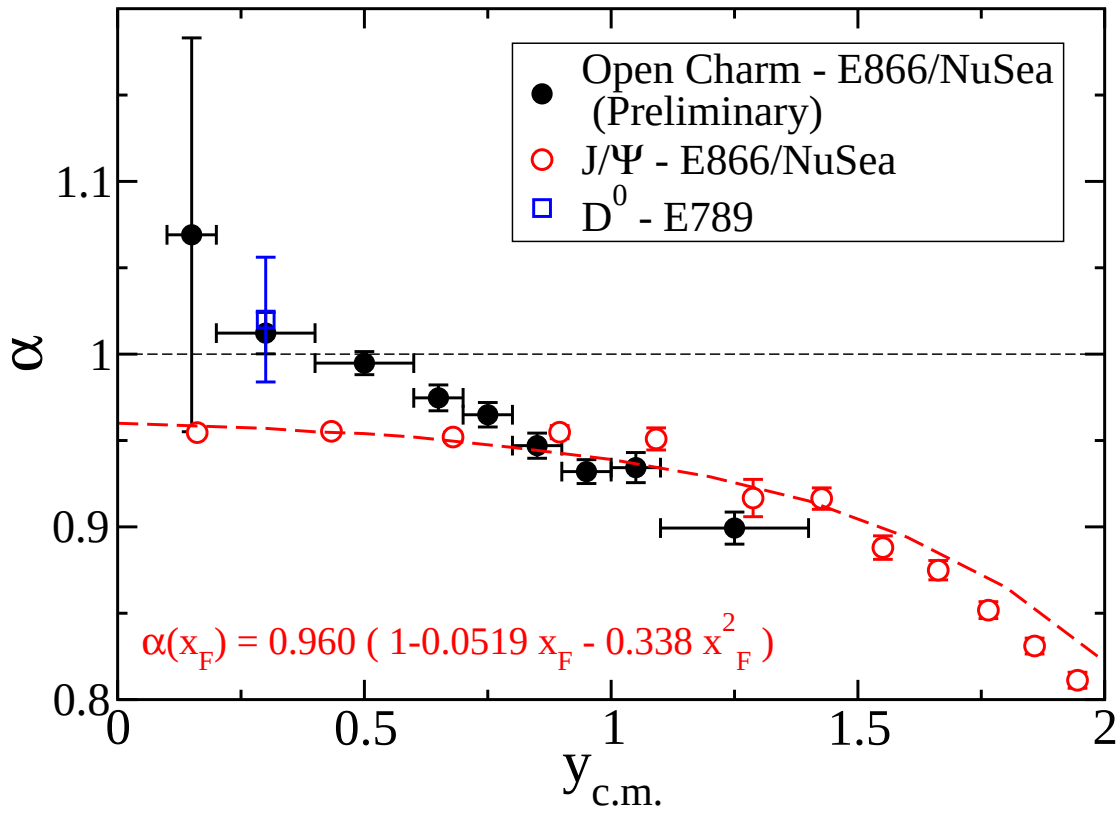

Figure 6: The J/ψ and open charm A dependence as a function of x_F (Mike Leitch).

Medium Effects

Nuclear effects often parameterized as

$$\sigma_{pA} = \sigma_{pp} A^{\alpha} \qquad \alpha(x_F, p_T)$$

For $\sqrt{s_{NN}} \leq 40$ GeV and $x_F > 0.25$, α decreases strongly with x_F – only low x_F effects probed by SPS and RHIC rapidity coverage

Possible cold matter effects

- **Nuclear Shadowing — initial-state effect on the parton distributions affecting total rate, important as a function of y/x_F**
- **Energy Loss — *either* initial-state effect, elastic scatterings of projectile parton before hard scattering creating quarkonium state, need to study Drell-Yan production to get a handle on the strength when shadowing is included — *or* final-state effect, scattering of the $c\overline{c}$ or J/ψ after production — can also be related to p_T broadening**
- **Intrinsic Charm — initial-state effect, if light-cone models correct, should only contribute to forward production, assumed to have different A dependence than normal J/ψ production**
- **Absorption — final-state effect, after $c\overline{c}$ that forms the J/ψ has been produced, pair breaks up in matter due to interactions with nucleons**

Shadowing

Parton Densities Modified in Nuclei

Nuclear deep-inelastic scattering measures quark modifications directly

More uncertainty in nuclear gluon distribution, only indirectly constrained by Q^2 evolution of parton densities

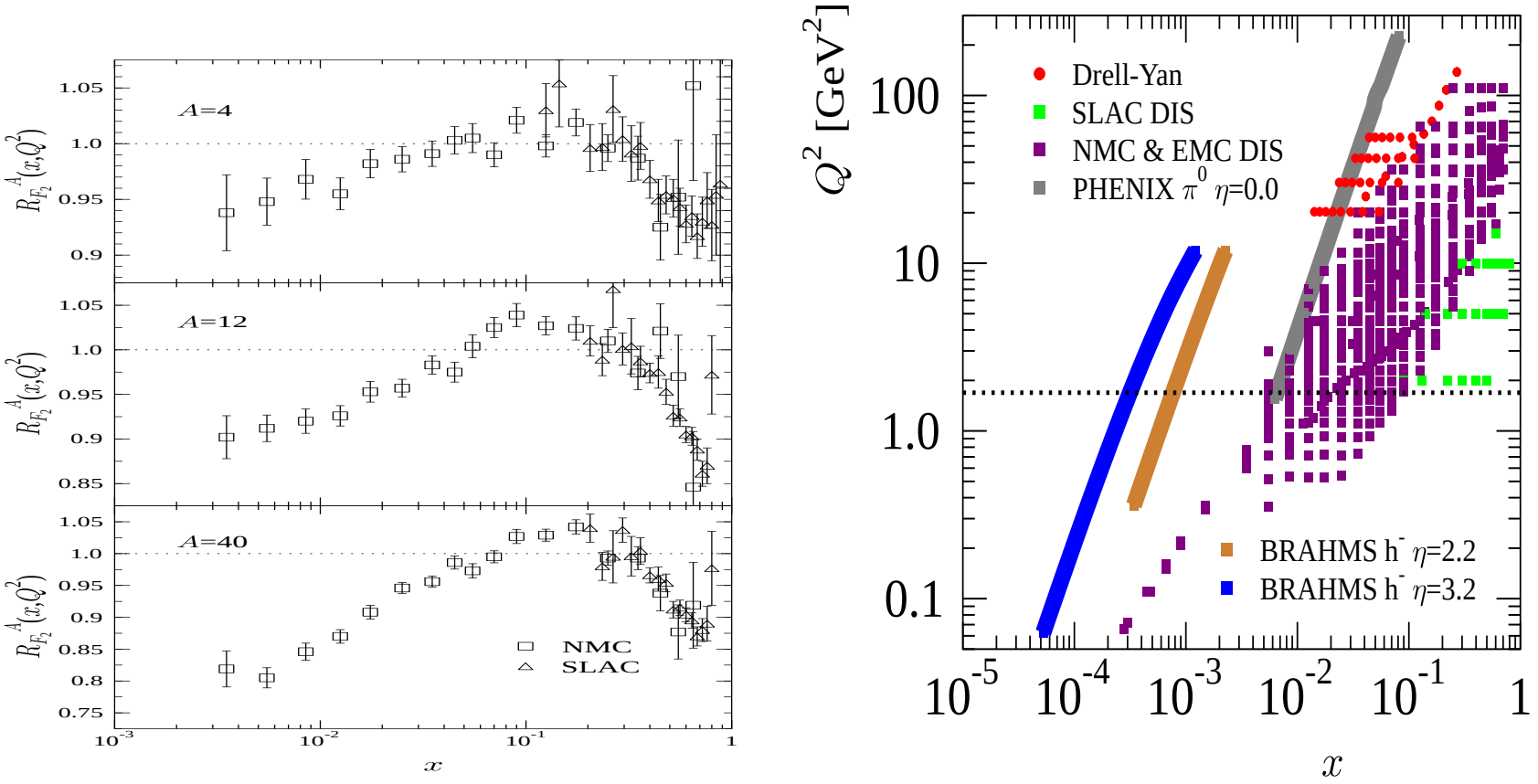

Figure 7: (Left) Ratios of charged parton densities in He, C, and Ca to D as a function of x. (Right) The x and Q^2 reach of present data used in nPDF fits. [From K.J. Eskola.]

x and Q^2 Reach of Heavy Ion Machines

p+Pb Collisions at the LHC are a factor of 25 higher energy than d+Au at RHIC, allowing broader range of cold matter studies in x and Q^2 than ever before

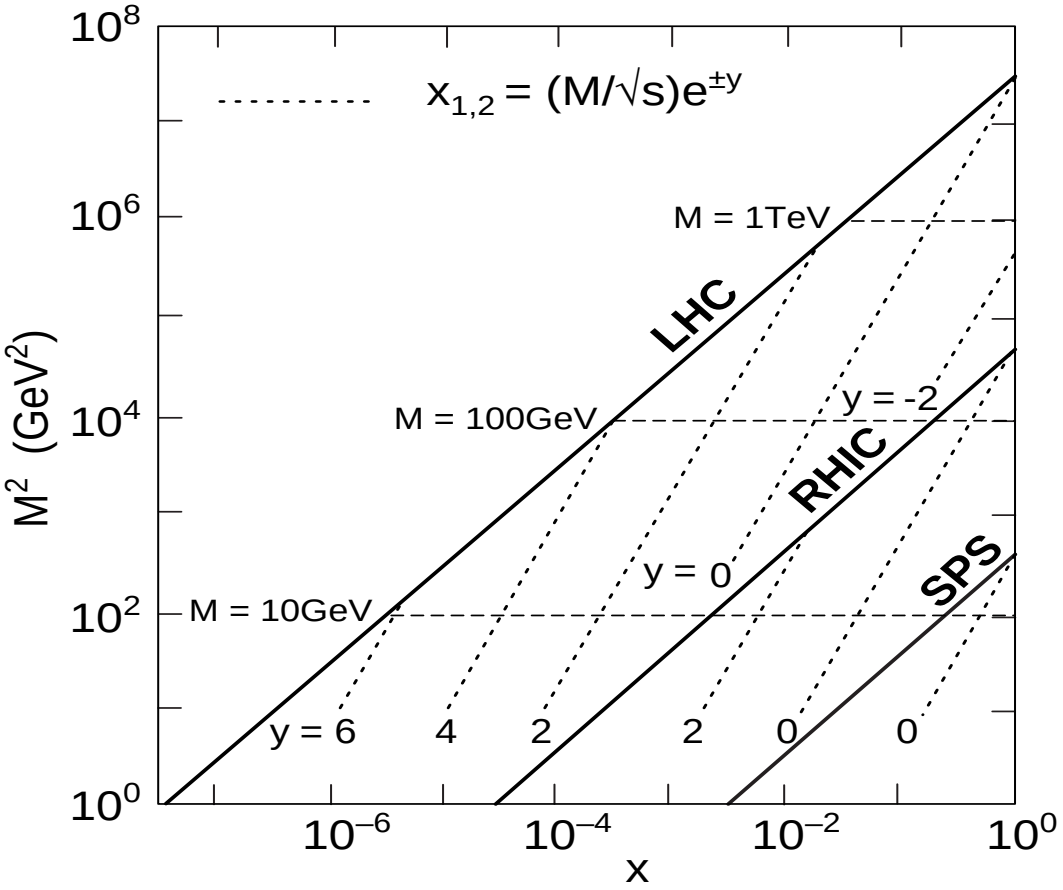

Figure 8: The Q^2 reach as a function of x for the SPS, RHIC and the LHC. Lines of constant rapidity are indicated for each machine.

Comparison of LO and NLO nDS nPDFs

When data are available, LO and NLO shadowing results agree, as they are meant to by construction

More tricky for the nuclear gluon density since it is not as well constrained

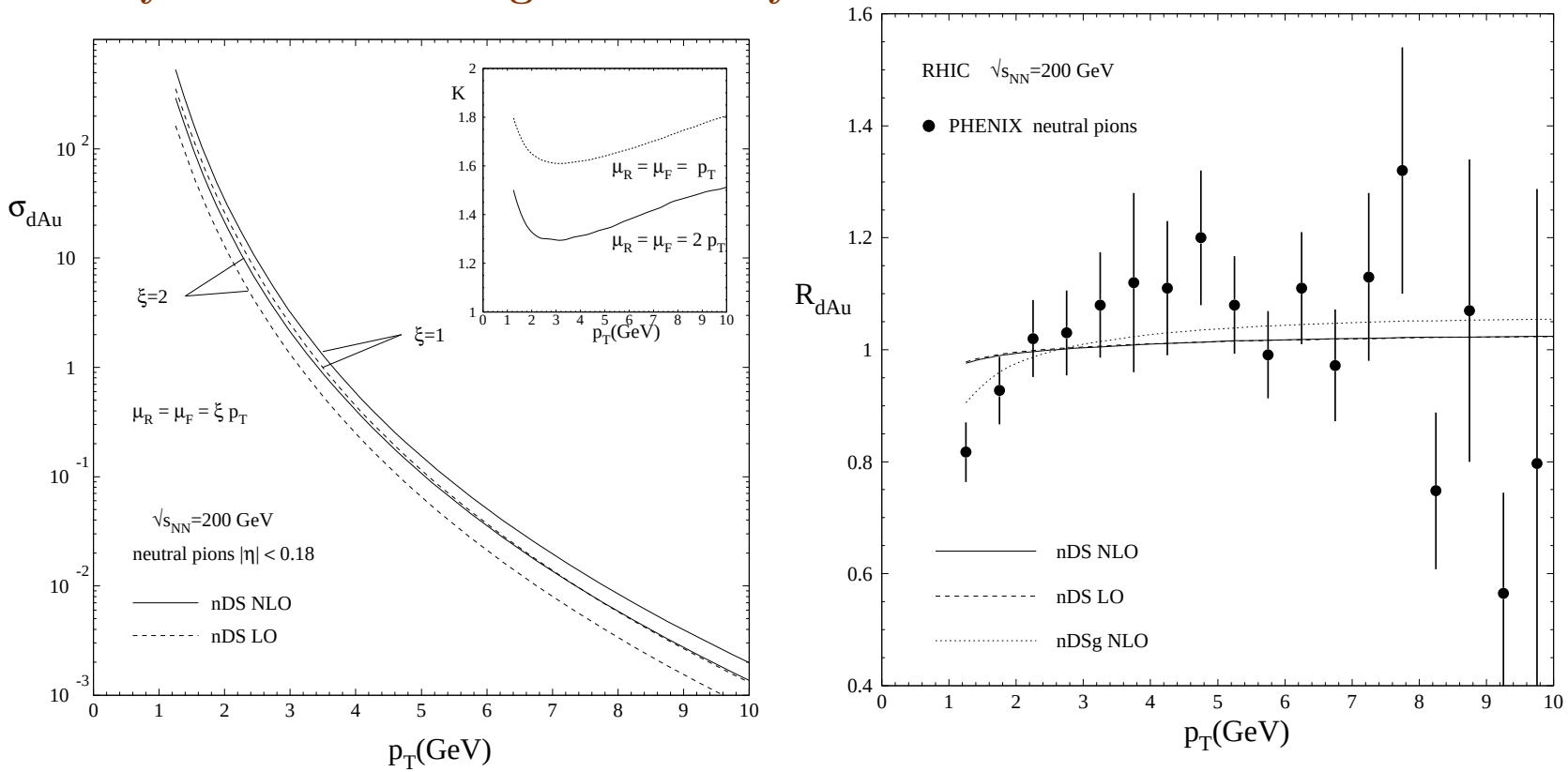

Figure 9: **(Left) The π^0 cross section in d+Au collisions at $\sqrt{s_{NN}} = 200$ GeV at LO and NLO. (Right) The LO and NLO calculations of $R_{\rm dAu}$, along with the NLO calculation with nDSg.**

Pinning Down the Gluon nPDF

To constrain gluon density using the J/ψ, also necessary to constrain other cold matter effects, left side shows NMC Sn/C J/ψ ratios, intermediate x only, not very conclusive

Right side: LO and NLO EPS09 shadowing ratios extracted from Q^2 evolution of nDIS; PHENIX π^0 data and momentum sum rules

LO ratios show wider antishadowing and bigger uncertainty in EMC region ($x > 0.3$), bigger uncertainty at low x

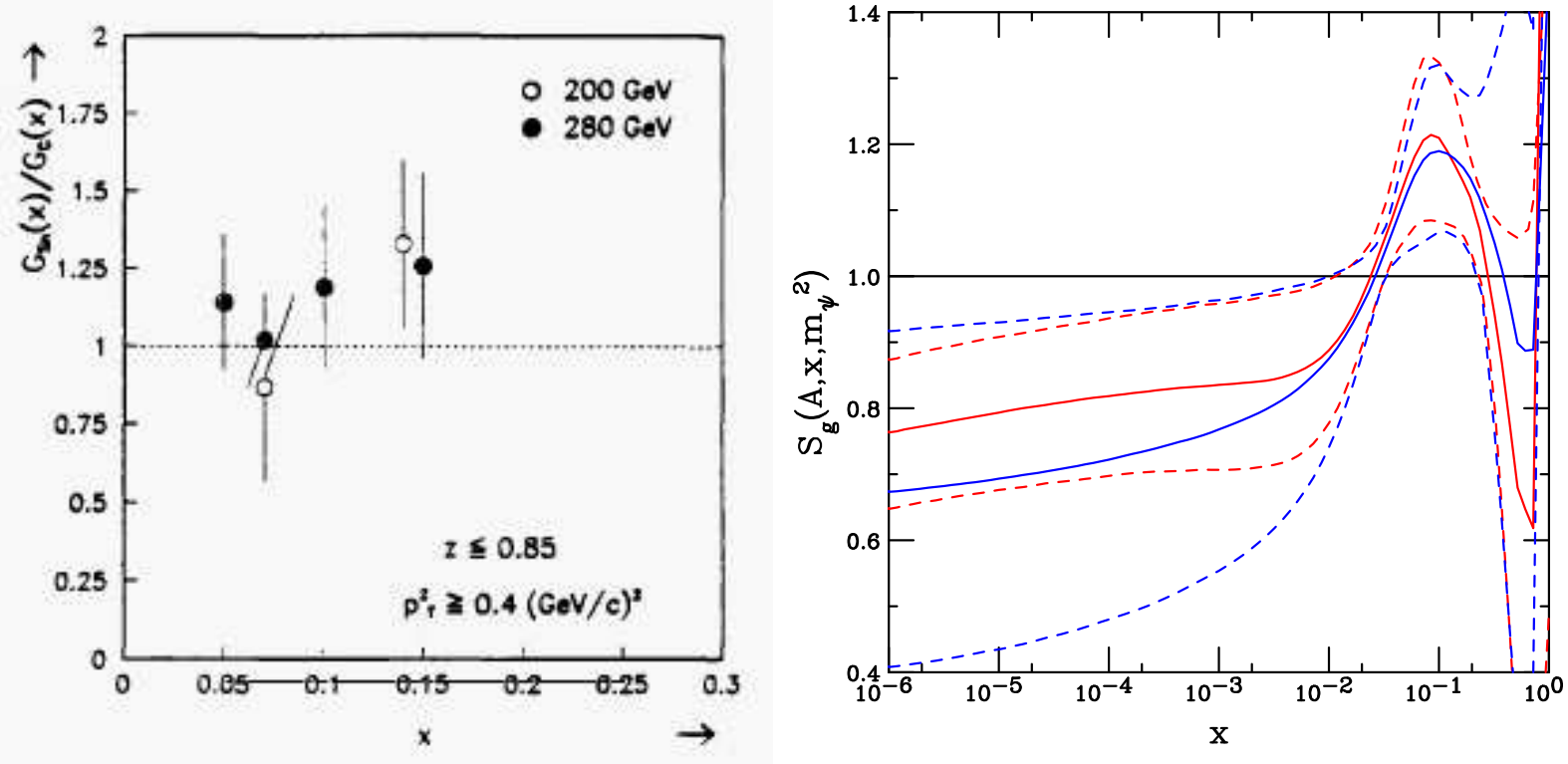

Figure 10: **(Left) Ratio of gluon distributions in Sn and C targets extracted from J/ψ production by NMC. (Right) The modification of the gluon densities at LO (blue) and NLO (red) with EPS09, including uncertainties (dashed lines), calculated at m_ψ.**

Shadowing on J/ψ in d+Au Collisions at $\sqrt{s_{NN}} = 200$ GeV

Left: $R_{\rm dAu}$ calculated at LO and NLO in CEM, Right: 'intrinsic' (LO CEM) vs. 'extrinsic' (LO CSM).

LO CEM calculation on left equivalent to 'intrinsic' $2 \to 1$ calculation with $p_T = 0$ on right-hand side

NLO CEM has higher average scale, shifts antishadowing peak to higher rapidity, and smaller scale dependence, similar to 'extrinsic' $2 \to 2$ LO CSM calculation

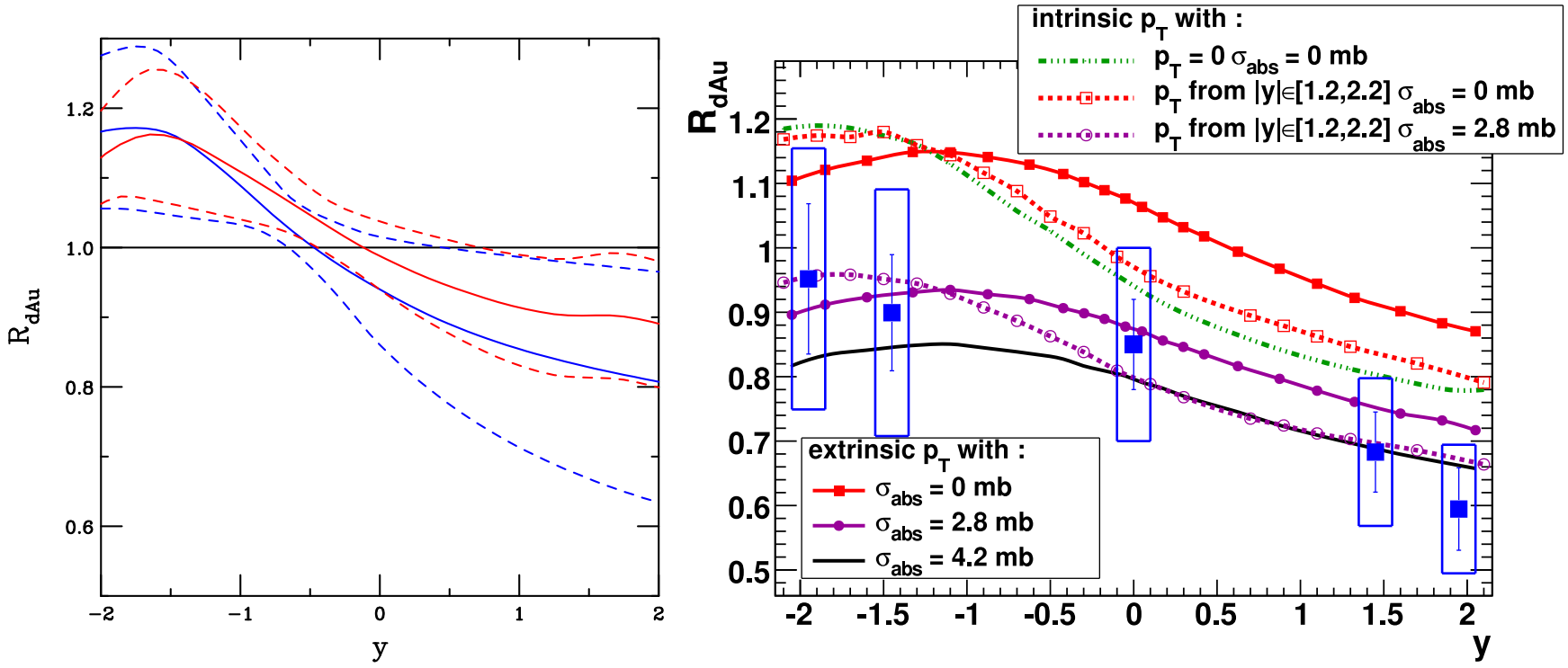

Figure 11: **Left: The LO and NLO calculations of $R_{\rm dAu}$. Right: 'Intrinsic' (CEM) vs. 'extrinsic' (CSM with s-channel cut) calculation of Ferreiro *et al.*.**

Saturation?

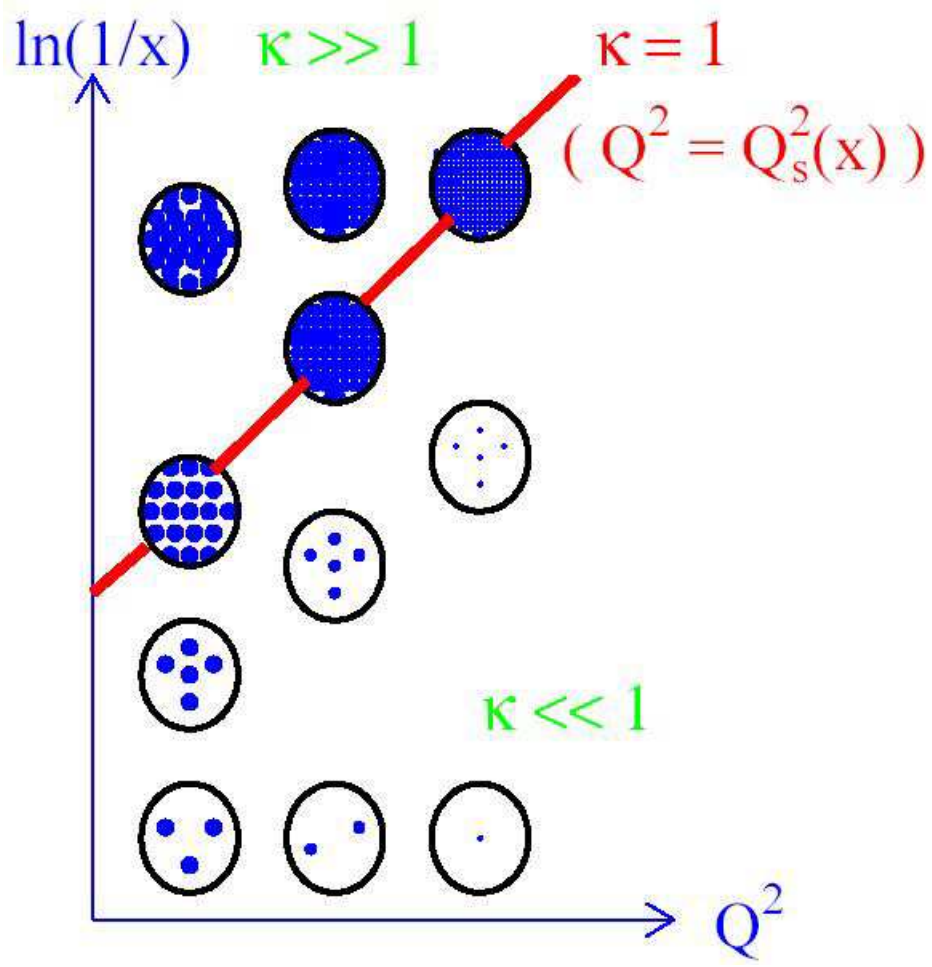

Saturation condition: when the gluon density, ρ_g, is sufficiently high, recombination of gluons $(2 \to 1)$ competes with emission of new partons $(1 \to 2)$ $\rho \sim 1/\alpha_s$

Packing factor: fraction of how much of nucleon/nuclear disk is packed with partons,
$\kappa = \sigma_{\rm dipole}/\pi R^2$, $\sigma_{\rm dipole} \propto F_2(x, Q^2)/Q^2$

$Q_{\rm sat}$ grows with increasing $\sqrt{s}$ and decreasing x

In nuclei $Q_{\rm sat}$ increases by $A^{1/3}$

Unclear whether or not J/ψ scale $\sim Q_{\rm sat}$

J/ψ A Dependence vs. x_2 and $y_{\rm cm}$

Effective α dissimilar as a function of x_2, closer to scaling for $y_{\rm cm}$

At negative x_F, the HERA-B result suggests a neglible effective J/ψ absorption crosss section

Argument for more physics at forward x_F than accounted for by nuclear shadowing

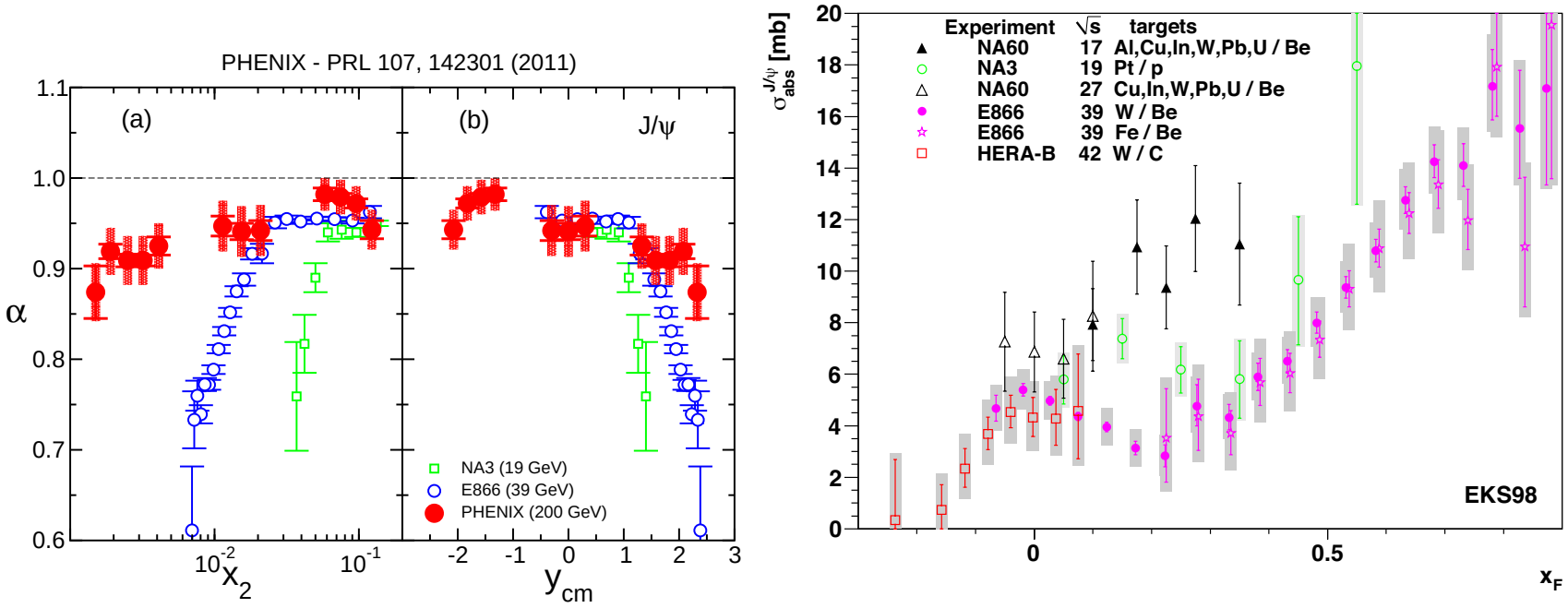

Figure 12: (Left) Comparison of effective α for NA3, E866 and PHENIX. (Mike Leitch) (Right) Comparison of effective $\sigma_{\rm abs}$ for J/ψ (from QWG report, 2010).

Energy Loss

Drell-Yan Production: Simplest Case

Good theory for pp production, small K factor at NLO, *if energy loss occurs in the initial state, it should be detectable in DY*

$K = 1.124 \pm 0.007$, $\chi^2/\mathrm{ndf} = 1.4$ **relative to E866 measurements in 800 GeV pp collisions (J.C. Webb Ph.D. thesis [arXiv:hep-ex/0302019]).**

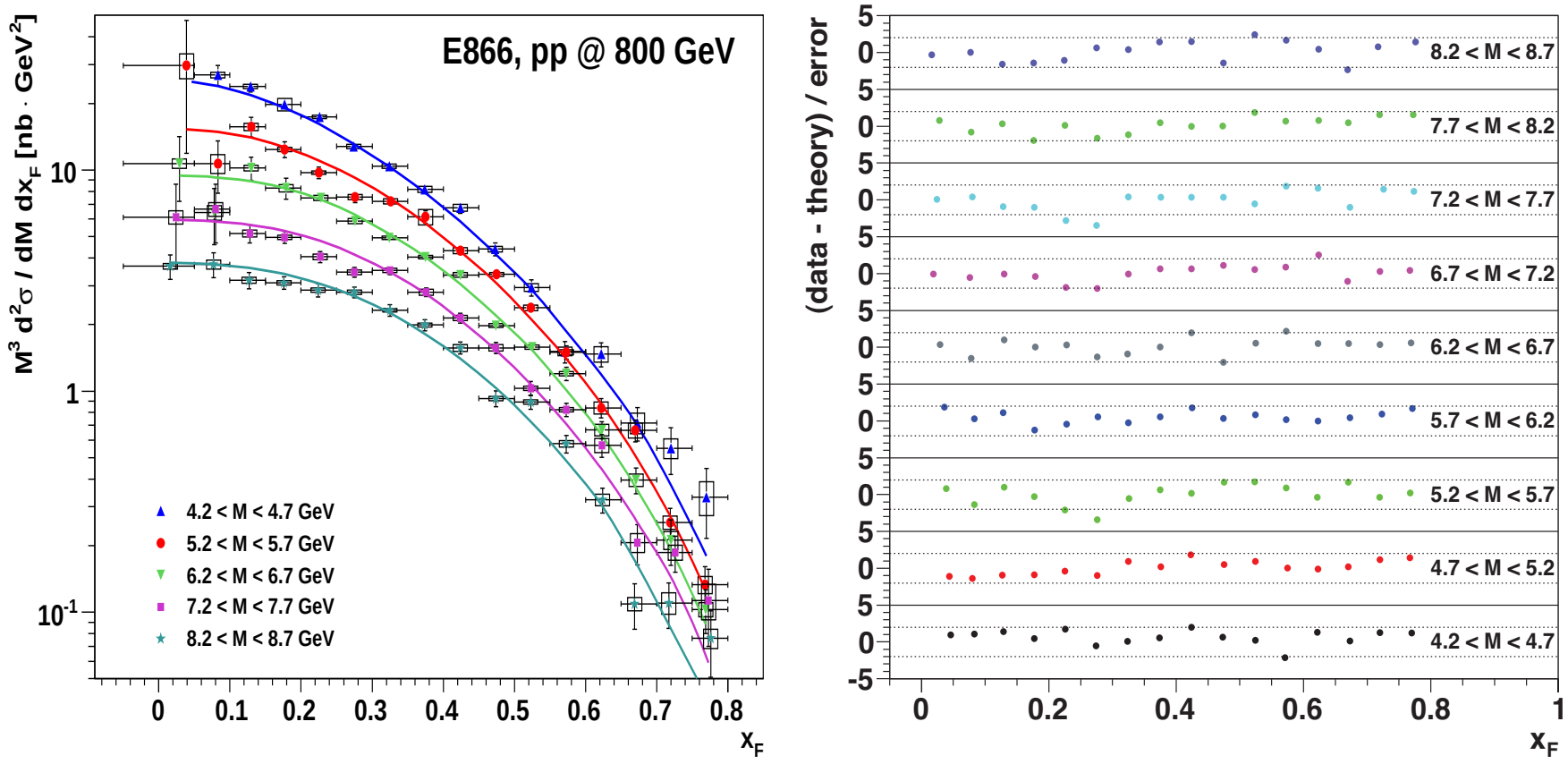

Figure 13: Left: The x_F dependence of the Drell-Yan cross section in several mass bins from 800 GeV pp colisions compared to NLO calculations. Right: Difference between the measured Drell-Yan cross section and the NLO calculations in the same mass bin.

Energy Loss in Drell-Yan? NA3 p+Pt at 400 GeV

Compare NA3 data with NLO calculations with/without central EPS09 nPDFs (difference small)

Test parameterization of initial state energy loss

$$x_1' = x_1(1-\epsilon_q)^{N-1}$$

x_1' enters $M^2 = x_1' x_2 s_{_{NN}}$, x_1 is in nPDFs, N is number of NN collisions, $\propto A^{1/3}$

Vary ϵ_q to get best fit, 99% confidence level gives upper limit on ϵ_q of 0.0020

Assume $\epsilon_g = (9/4)\epsilon_q$ for NLO qg contribution

$K \sim 1$, χ^2/ndf slightly smaller with no shadowing

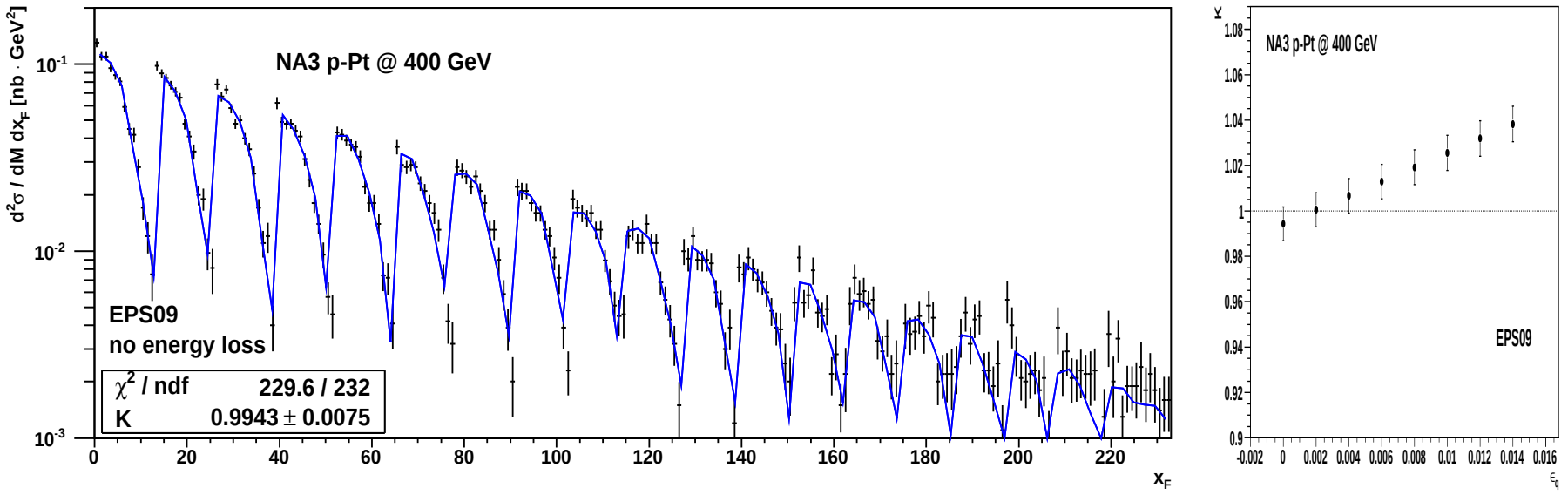

Figure 14: Left: The invariant DY cross section in pPt collisions at 400 GeV as a function of x_F in different mass bins with EPS09 nPDFs. Right: The K factors found in comparison to the data with various values of the energy loss parameter ϵ_q.

Is Shadowing Sufficient to Explain Data?

Extracting energy loss from shadowing difficult, the two are intertwined

At 400 GeV and $4 < M < 9$ GeV, the modification of the Drell-Yan cross section is nearly independent of x_F, thus energy loss extracted from data is basically independent of EPS09 PDFs; average K factor shift can account for difference

E866 W/Be and Fe/Be ratios at 800 GeV in similar mass regions suggest energy loss parameter no larger than that found at 400 GeV; E772 W/D and Fe/D ratios confirm trend

Is energy loss a predominantly final-state effect? Then Drell-Yan is unaffected...

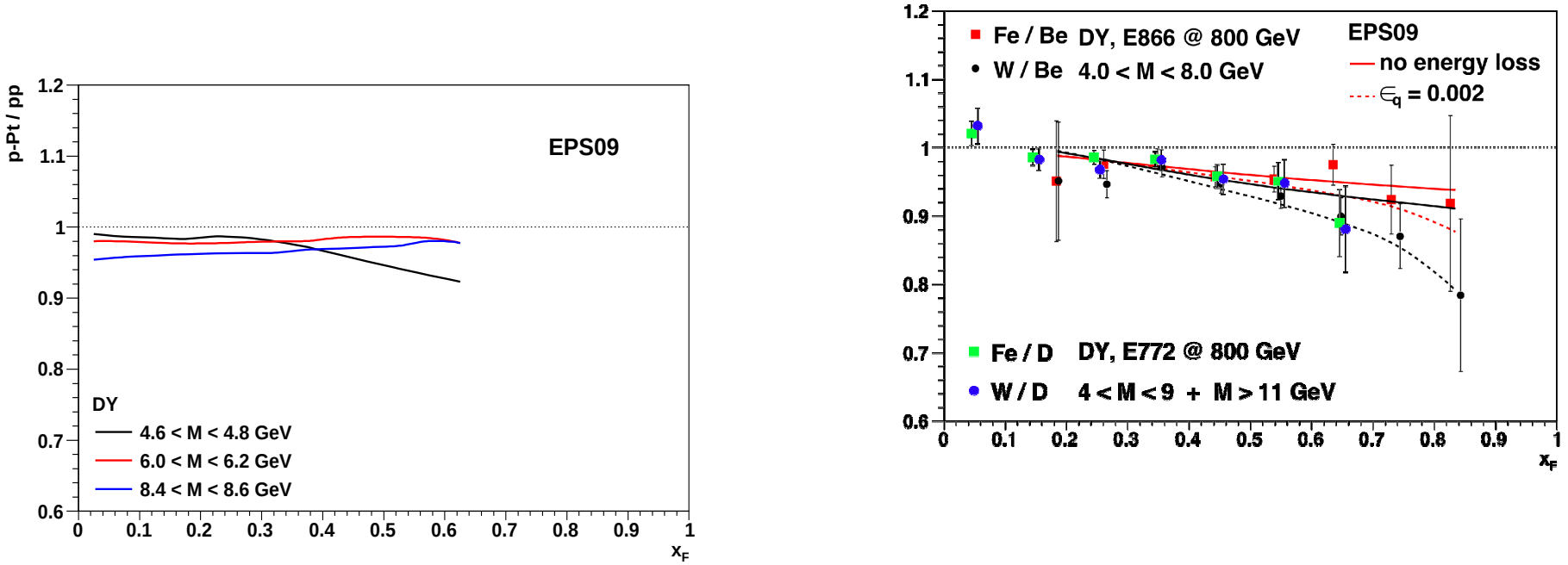

Figure 15: Left: The 400 GeV pPt/pp ratio for Drell-Yan production in several different mass bins as a function of x_F with the central EPS09 nPDF. Right: Heavy-to-light ratios for Drell-Yan production at 800 GeV. The curves show the EPS09 results with no energy loss included (solid) and $\epsilon_q = 0.0020$ (dashed) the same value obtained at 400 GeV. The Fe/Be ratio, similar to Fe/D, is shown in red while the W/Be (W/D) ratios are shown in black. (Note that these curves

Other DY Energy Loss Calculations

Left-hand side shows limits on energy loss in different cases (fitting schematic parameters k_1, k_2 and k_3 to E866 DY data):

Gavin and Milana (PRL 68, 1834 (1992)), $\Delta x_1 = -k_1 x_1 A^{1/3}$

Brodsky and Hoyer (PL B 298, 165 (1993)), $\Delta x_1 = -(k_2/s)A^{1/3}$

Baier *et al* **(NP B 484, 265 (1997); 531, 403 (1998)),** $\Delta x_1 = -(k_3/s)A^{2/3}$

Right-hand side is calculation by Kopeliovich *et al* **(PRL 86, 4483 (2001)),** $dE/dx = 2.32 \pm 0.52 \pm 0.50$ **GeV/fm fit to E772 data**

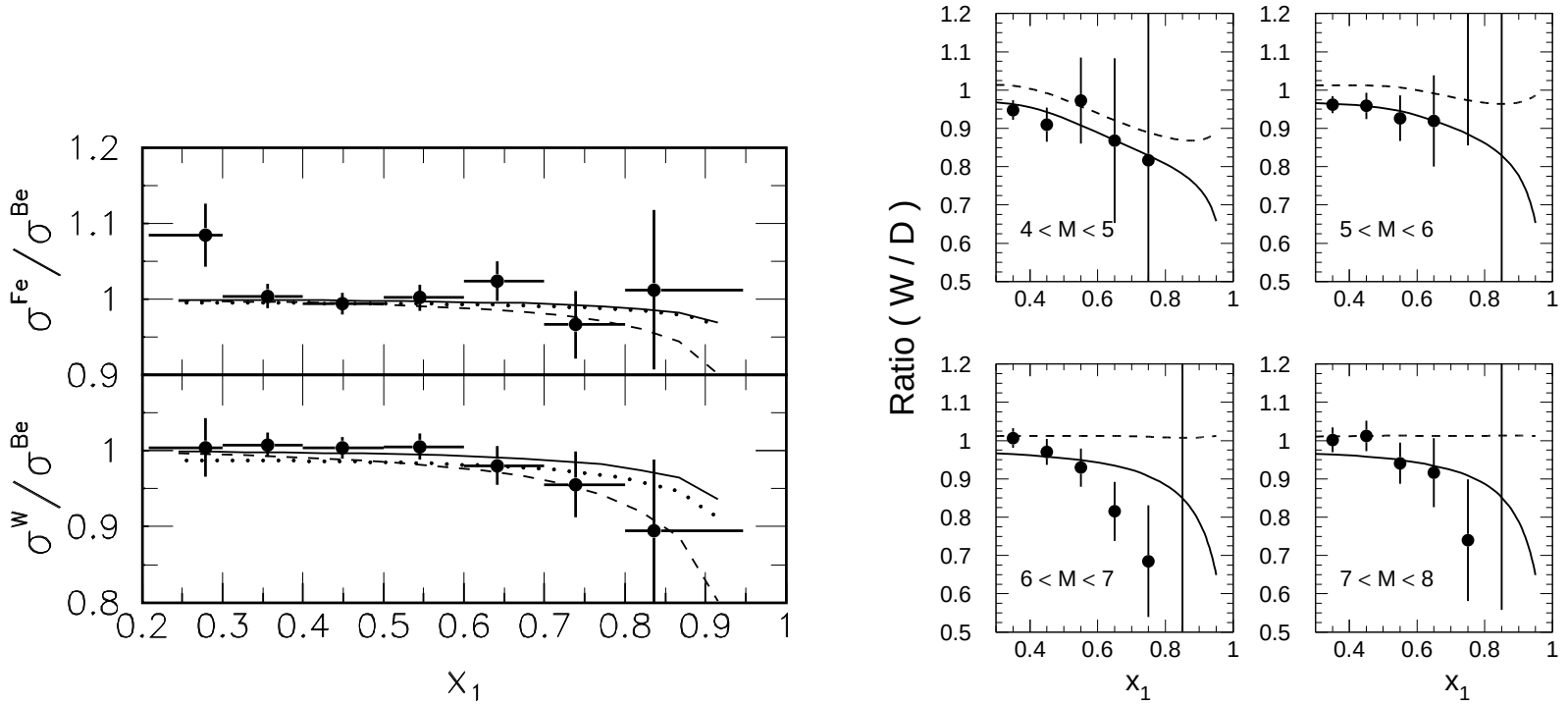

Figure 16: Left: Cross section ratios, Fe/Be and W/Be, calculated with energy loss, after E866 data correction for EKS98 shadowing. The dashed curve is the Gavin-Milana best fit while the dashed curve is the 1σ limit. The dotted curve is the upper limit on energy loss for the results with $\Delta x_1 \propto 1/s$. Right: Calculation of W/D ratio for a specific E772 mass bin, shadowing and energy loss are included in the result.

Adding Initial-State Energy Loss to J/ψ Production

Rather large EPS09 uncertainty reduced in ratios; clearly initial-state shadowing is insufficient to describe effect

Combination of shadowing and energy loss with relatively x_F-independent absorption compares relatively well with the data for $x_F > 0.2$; HOWEVER, the assumed ϵ_g is much larger than ϵ_q for Drell-Yan production – incompatible with initial-state energy loss but supports final-state loss

Stronger absorption closer to target? Formation time effects not included

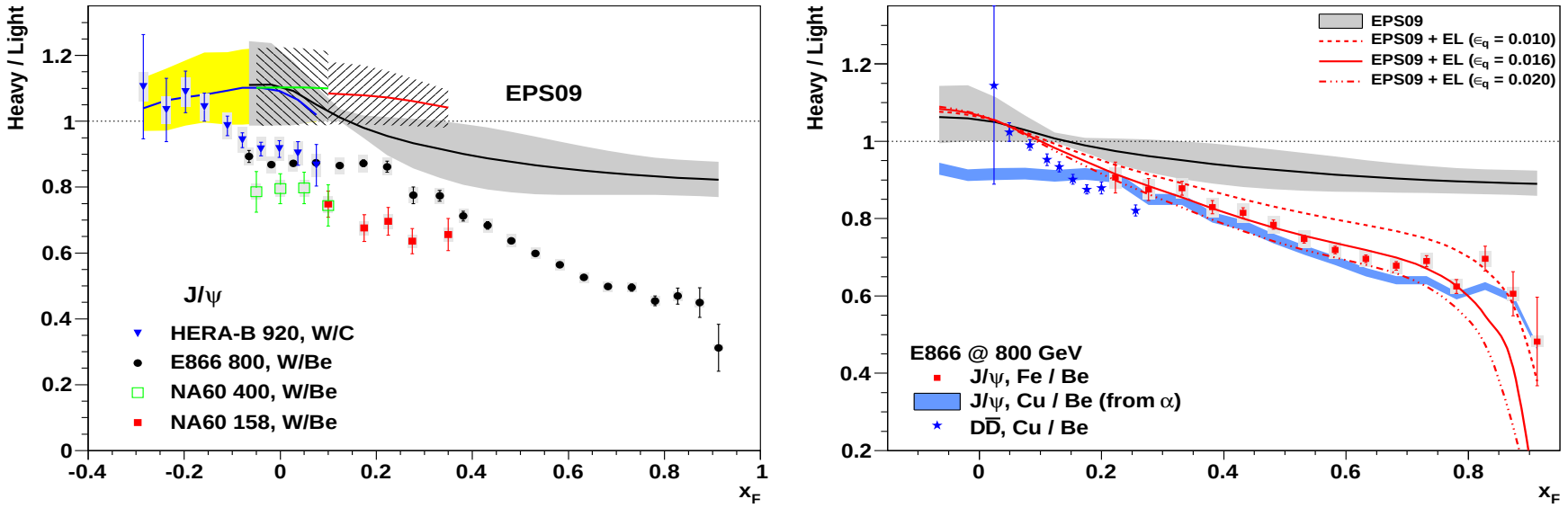

Figure 17: Left: The heavy to light ratios for W/Be in fixed target interactions. Right: Convolution of shadowing, absorption and various strengths of initial-state energy loss by quarks compared to the E866 data.

Final-State Energy Loss (Kharzeev and Satz)

Backward rise could be due to final-state energy loss

Kharzeev and Satz (Z. Phys. C 60, 389 (1993)), assumed final-state loss of color octet $c\bar{c}$, momentum is reduced by $\sim \kappa L_A$ where κ is string tension and L_A is path length, ψ state produced with x_F/δ where $\delta \approx 1 - \kappa L_A/P_\psi$

$$G_A(x_F) \propto S_A G_p(x_F) + (1 - S_A)\frac{G_p(x_F/\delta)}{\delta}\theta(1 - x_F/\delta)$$

Lower energies show a stronger decrease

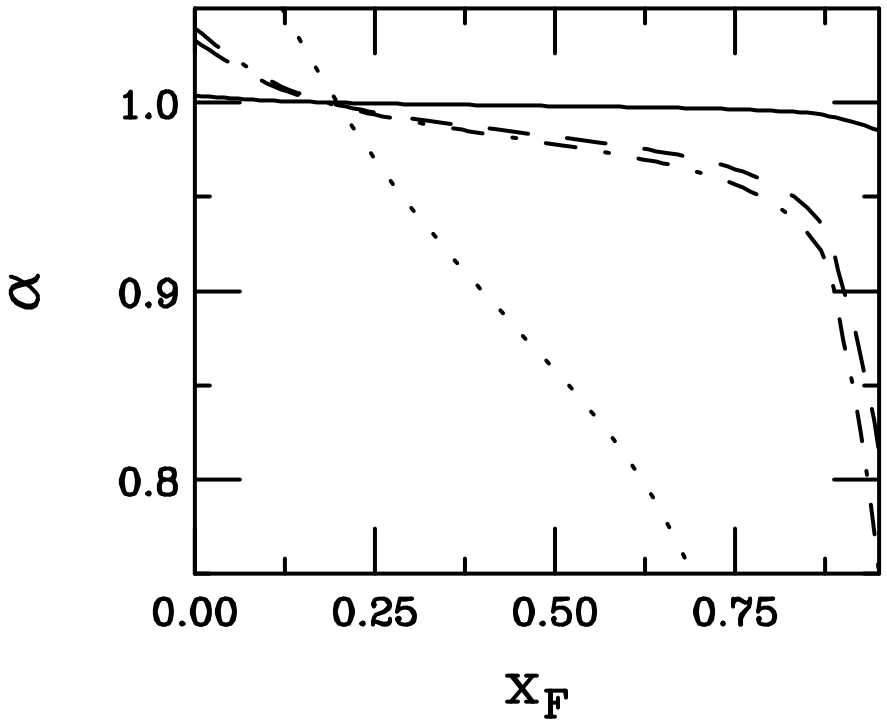

Figure 18: The A dependence of ψ production assuming KS loss for $x_F > 0$. Octet cross sections of 1 mb (solid), 20 mb (dashed) and 40 mb (dot-dashed) are calculated with the MRST LO parton densities at 800 GeV. At 120 GeV, a 40 mb octet cross section is assumed (dotted).

Final-State Energy Loss (Arleo and Peigne)

Arleo and Peigne (arXiv:1212.0434) fits an energy loss parameter that also depends on L_A to E866 data and uses the same parameter for other energies

$$\frac{1}{A}\frac{d\sigma_{pA}(x_F)}{dx_F} = \int_0^{E_p-E} d\epsilon P(\epsilon)\frac{d\sigma_{pp}(x_F+\delta x_F(\epsilon))}{dx_F}$$

The pp result is calculated without any particular production model, $d\sigma_{pp}/dx = (1-x)^n/x$ where n is fit to data, up to $n \sim 34$ at LHC energies

Backward x_F effect is large for this scenario

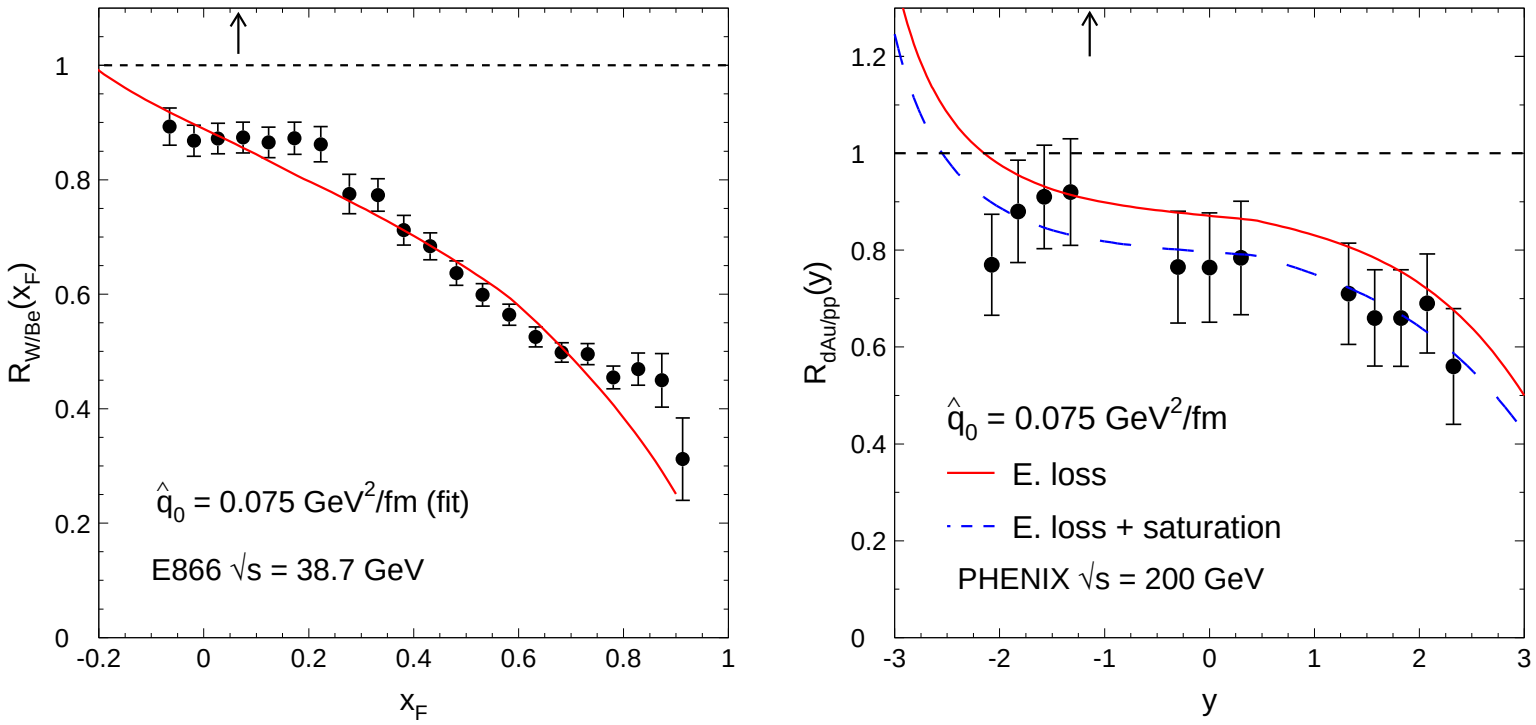

Figure 19: E866 J/ψ suppression in pW/pBe collisions at $\sqrt{s} = 38.8$ GeV (left) and the PHENIX $R_{\rm dAu}$ at $\sqrt{s} = 200$ GeV collisions (right) calculated by Arleo

Intrinsic Charm

Intrinsic Charm

Proton wavefunction can be expanded as sum over complete basis of quark and gluon states: $|\Psi_p\rangle = \Sigma_m \, |m\rangle \, \psi_{m/p}(x_i, k_{T,i}, \lambda_i)$

$|m\rangle$ are color singlet state fluctuations into Fock components $|uud\rangle$, $|uudg\rangle \cdots |uudc\overline{c}\rangle$

Boost invariant wavefunctions $\psi_{m/p}(x_i, k_{T,i}, \lambda_i)$ depend on $x_i = k_i^+/P^+$ and $k_{T,i}$ the momentum fraction and transverse momentum for each parton. Momentum conservation demands $\Sigma_{i=1}^n x_i = 1$ and $\Sigma_{i=1}^n \vec{k}_{T,i} = 0$, where n is the number of partons in Fock state $|m\rangle$

The intrinsic charm fluctuations can be freed by a soft interaction if the system is probed during the time $\Delta t = 2p_{\rm lab}/M^2_{c\overline{c}}$ that the fluctuations exist

Dominant Fock state configurations have minimal invariant mass, $M^2 = \Sigma_i \, m^2_{T,i}/x_i$, where $m^2_{T,i} = k^2_{T,i} + m^2_i$ is the squared transverse mass of parton i in the state; corresponds to configurations with equal rapidity constituents

Since intrinsic charm quarks have the same rapidity as other partons in the state, their larger mass gives them a higher momentum fraction than the comoving light partons

A Dependence of Intrinsic Charm

EMC analyses of EMC charm structure function data find $P_{\rm ic} \sim 0.3 - 1$ %

Intrinsic charm is stronger at lower energies because $\sigma_{\rm lt}$ is smaller but because $\sigma_{\rm ic}$ does not change much with energy, effect decreases as energy increases

Intrinsic charm dominates the A dependence at high x_F, note difference between projectile and target regions

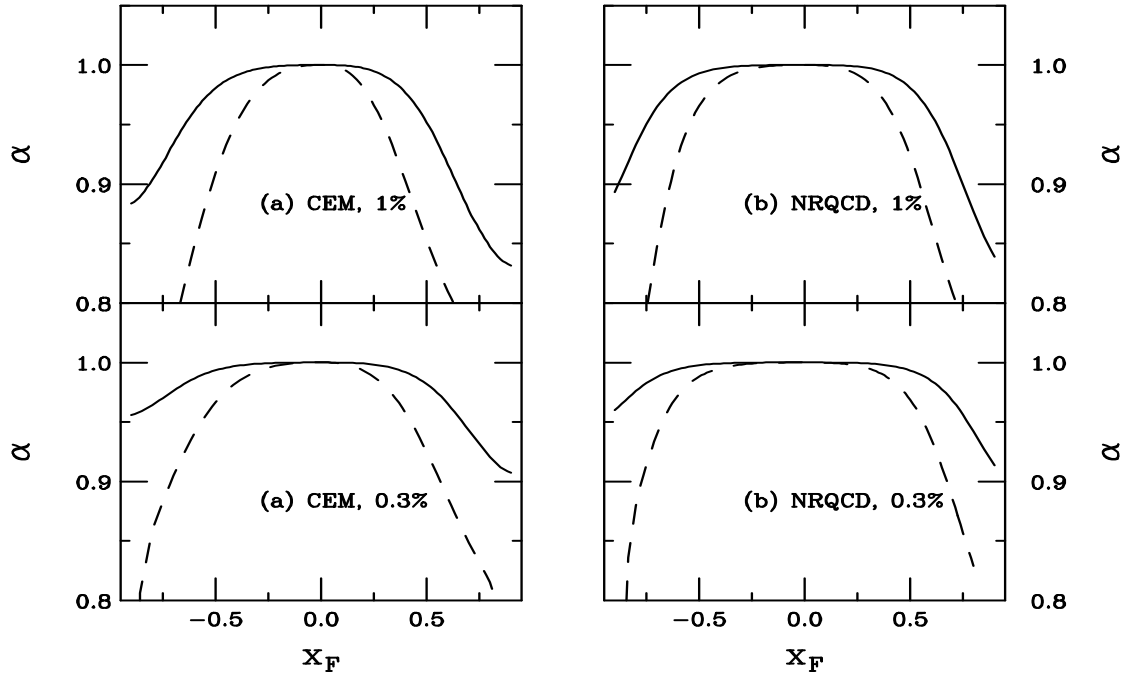

Figure 20: The A dependence of intrinsic charm at 800 GeV (solid) and 120 GeV (dashed). In (a) and (c) an effective production probability of 1% is assumed in the CEM and in NRQCD respectively while in (c) and (d) $P_{\rm ic}^{\rm eff} = 0.31\%$ is assumed in the CEM and in NRQCD. At $x_F > 0$ the projectile proton strikes a nuclear target, at negative x_F, the nuclear 'projectile' strikes a proton target, making the A dependence different in the two regions.

Nuclear Absorption

A Dependence of J/ψ and ψ' Not Identical

Extensive fixed-target data sets (NA50 at SPS, E866 at FNAL) show clear difference at midrapidity [NA50 ρL fit gives $\Delta\sigma = \sigma^{\psi'}_{\rm abs} - \sigma^{J/\psi}_{\rm abs} = 4.2 \pm 1.0$ mb at 400 GeV, 2.8 ± 0.5 mb at 450 GeV for absolute cross sections]

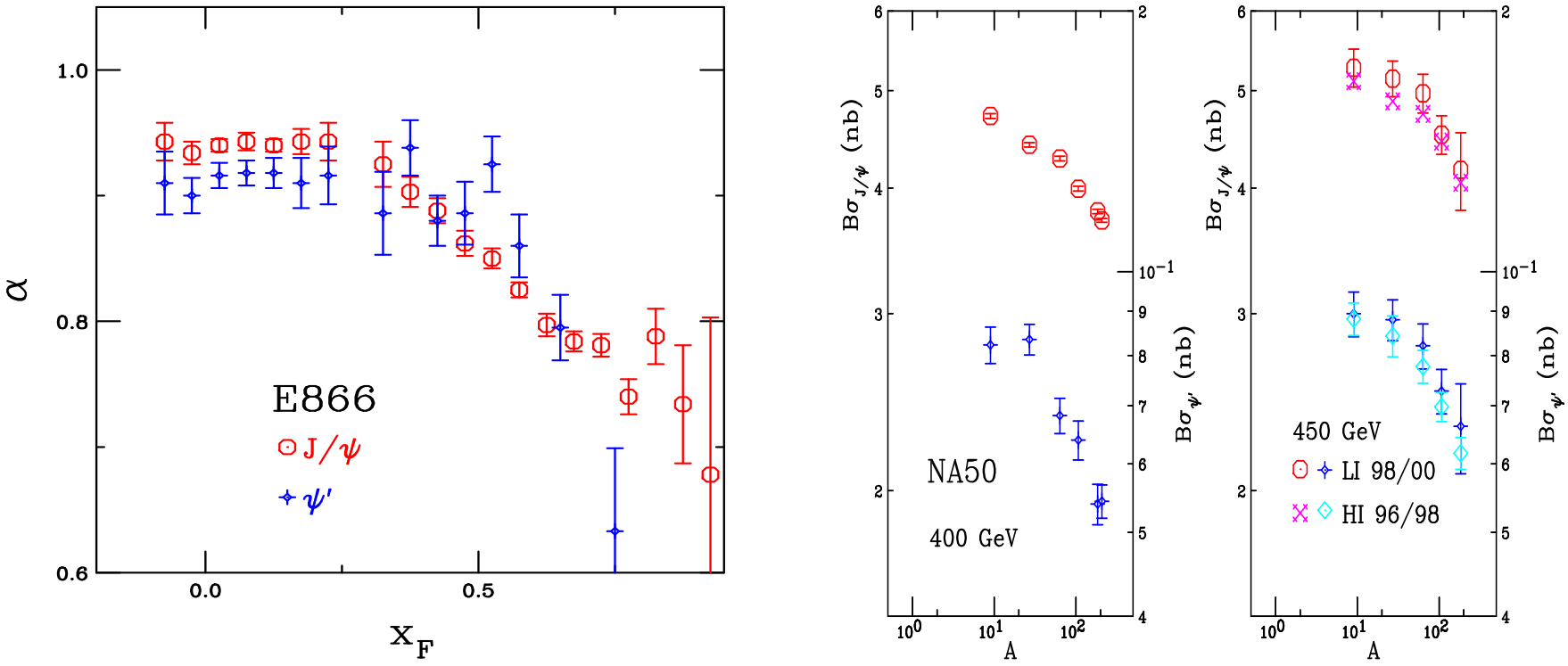

Figure 21: The J/ψ A dependence (left) as a function of x_F at FNAL ($\sqrt{S_{NN}} = 38.8$ GeV) and (right) and a function of A at the SPS (NA50 at $p_{\rm lab} = 400$ and 450 GeV) for J/ψ and ψ' production.

PHENIX Has Measured $R_{\rm dAu}$ for ψ' and χ_c

First results shown at Quark Matter '12 for ψ' and χ_c

$R_{\rm dAu} \sim 0.75 \pm 0.20, 0.75 \pm 0.25, 0.30 \pm 0.15$ **for J/ψ, χ_c and ψ' respectively**

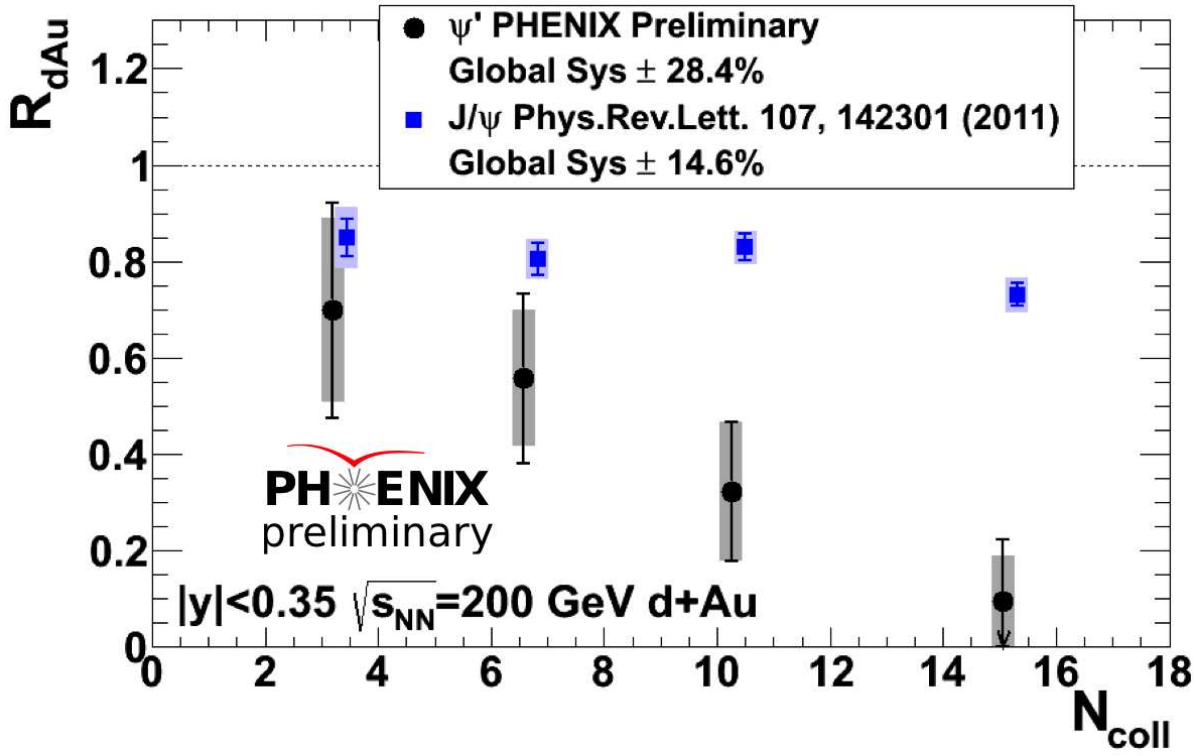

Figure 22: The J/ψ and ψ' $N_{\rm coll}$ dependence as reported by PHENIX at QM'12 by D. McGlinchey.

A Dependence of Charmonium States May Differ

NRQCD approach predicts different cross sections for J/ψ, ψ' and χ_c

$$\frac{d\sigma_{pA}^{\psi,\,\mathrm{tot}}}{dx_F} = \left[\frac{d\sigma_{pp}^{\psi,\,\mathrm{dir,\,oct}}}{dx_F} + \sum_{J=0}^{2} B(\chi_{cJ} \to \psi X)\frac{d\sigma_{pp}^{\chi_{cJ},\,\mathrm{oct}}}{dx_F} + B(\psi' \to \psi X)\frac{d\sigma_{pp}^{\psi',\,\mathrm{oct}}}{dx_F}\right] \int d^2b T_A^{\mathrm{eff\,(oct)}}(b)$$
$$+ \int d^2b \left[\frac{d\sigma_{pp}^{\psi,\,\mathrm{dir,\,sing}}}{dx_F} T_A^{\psi,\mathrm{dir,eff\,(sing)}}(b) + \sum_{J=0}^{2} B(\chi_{cJ} \to \psi X)\frac{d\sigma_{pp}^{\chi_{cJ},\,\mathrm{sing}}}{dx_F} T_A^{\chi_{cJ},\,\mathrm{eff\,(sing)}}(b) + B(\psi' \to \psi X)\frac{d\sigma_{pp}^{\psi',\,\mathrm{sing}}}{dx_F} T_A^{\psi',\,\mathrm{eff\,(sing)}}(b)\right]$$

$$T_A^{\mathrm{eff}}(b) = \int_{-\infty}^{\infty} dz\, \rho_A(b,z) \exp\left\{-\int_z^{\infty} dz' \rho_A(b,z')\sigma_{\mathrm{abs}}(z'-z)\right\}$$

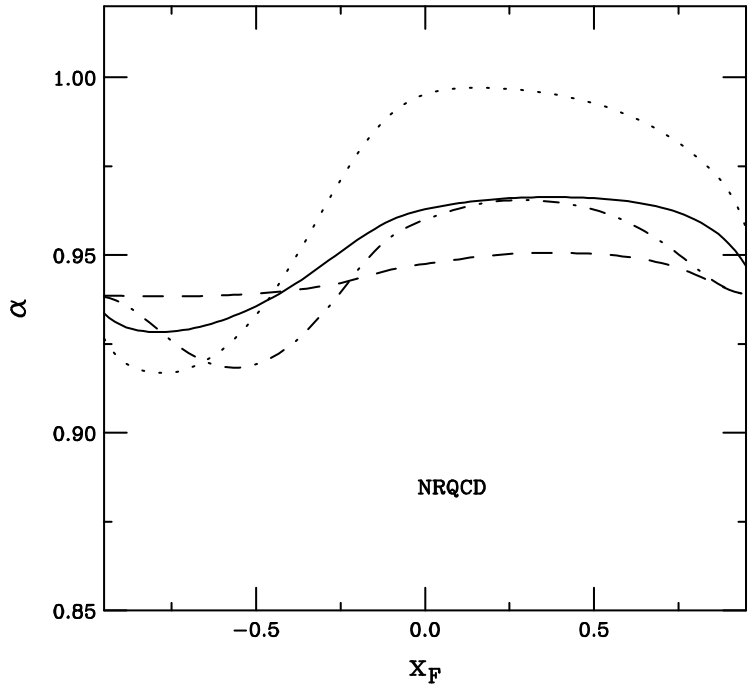

Figure 23: The A dependence of singlet and octet absorption is shown at 920 GeV. The total J/ψ dependence is given in the solid curve, the direct J/ψ in the dashed, ψ' in the dot-dashed, and χ_c in the dotted curve assuming $\sigma_{\mathrm{abs}}^{\mathrm{octet}} = 4$ mb and $\sigma_{\mathrm{abs}}^{\mathrm{singlet}\,J/\psi} = 5$ mb.

Effective Absoprtion Cross Section Energy Dependent

Once data corrected for shadowing effects, dependence of effective absorption cross section on center of mass energy is clear

In backward region, quarkonium states should be fully formed within the target

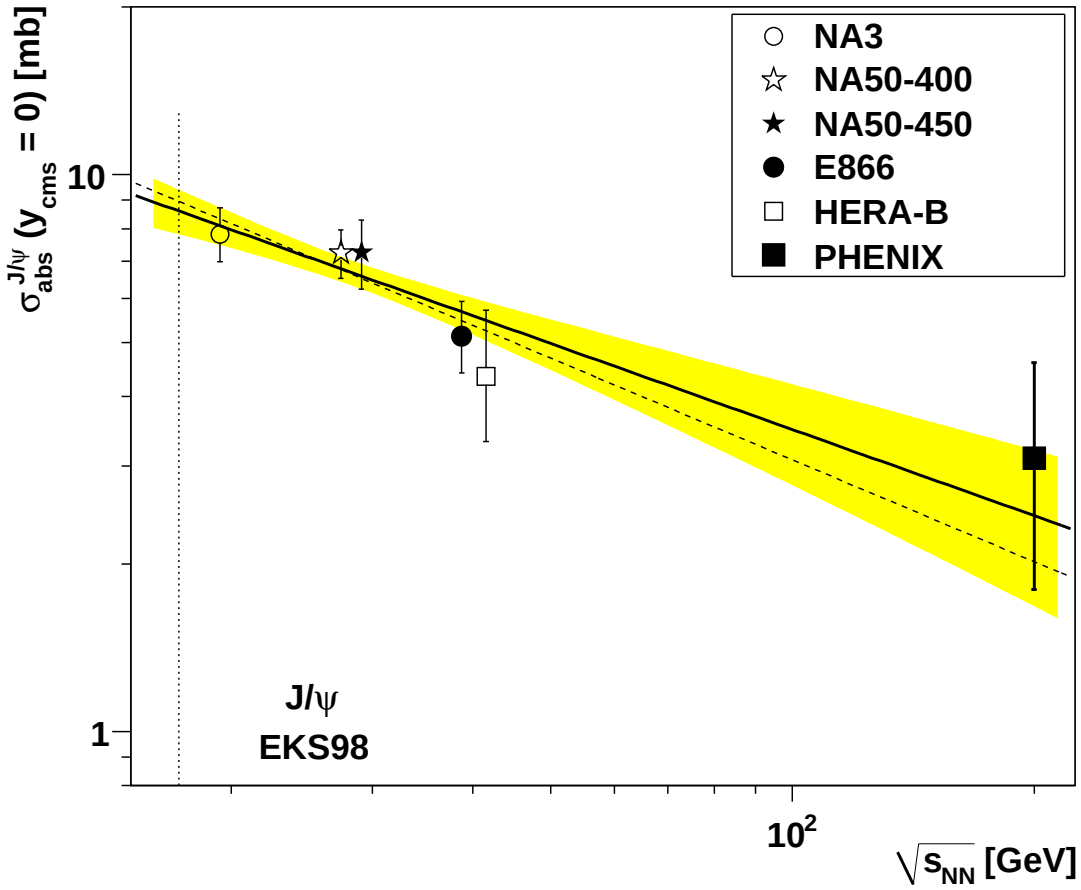

Figure 24: At midrapidity, the effective absorption cross section decreases as a function of energy. (Modified from Lourenco, Wohri and RV.)

Summary .

- **Lots of interesting nuclear effects on open charm and charmonium**
- **Rapidity/x_F dependence of J/ψ production not yet well understood in pA/d+Au**
- **LHC p+Pb collisions at $\sqrt{s} = 5$ TeV could provide some surprises**
- **Υ measurements, not discussed here, give another handle on understanding cold nuclear matter effects on quarkonium**